Potential fluctuations and energetic ion production in hollow cathode discharges

Dan M. Goebel,[a] Kristina K. Jameson, Ira Katz, and Ioannis G. Mikellides
Jet Propulsion Laboratory, California Institute of Technology, 4800 Oak Grove Drive, Pasadena, California 91109, USA

Ions with energies significantly in excess of the applied discharge voltage have been reported for many years in hollow cathode discharges. Models of dc potential hills downstream of the cathode and instabilities in postulated double layers in the cathode orifice have been proposed to explain this, but have not been substantiated. Measurements of the dc and rf plasma density and potential profiles near the exit of hollow cathodes by miniature fast-scanning probes suggests that turbulent ion acoustic fluctuations and ionization instabilities in the cathode plume significantly increase the energy of the ions that flow from this region. Increases in the discharge current and/or decreases in the cathode gas flow enhance the amplitude of the fluctuations and increase the number and energy of the energetic ions, which increases the erosion rate of the cathode electrodes. The transition from the quiescent "spot mode" to the noisy "plume mode" characteristic of these discharges is found to be a gradual transition of increasing fluctuation amplitudes. © *2007 American Institute of Physics*. [DOI: 10.1063/1.2784460]

I. INTRODUCTION

Hollow cathodes have been used in many applications to produce plasma for ion sources, thrusters, lasers, plasma processing, etc. Hollow cathodes can be generically described as having an active electron-emitting surface or insert inside of a hollow refractory metal tube, typically with an orifice plate welded to the downstream end, as illustrated schematically in Fig. 1. Neutral gas is injected through the tube, and electrons emitted from the insert generate plasma inside the cathode from which plasma electrons are extracted through the orifice to produce the main discharge to an exterior anode. The primary purpose of enclosing the electron emitter surface inside the hollow structure is to increase the neutral density in the insert region to reduce the ion energy bombarding the thermionic emitter that can damage the surface and degrade the work function.[1] The hollow cathode structure normally has a heating element wrapped around the cathode tube that is heat shielded, and is often enclosed inside another electrode called the keeper. The keeper, also shown in Fig. 1, is an insulated hollow tube with a slightly larger orifice on the end that is aligned with the cathode aperture. The purpose of the keeper is to draw a small amount of current from the cathode to facilitate turn-ON, to draw sufficient "keep-alive" current to maintain the cathode temperature if the main discharge current is turned off or interrupted, and to protect the cathode orifice plate and heater from ion bombardment and erosion by the main discharge plasma. However, significant erosion of the cathode keeper by ion bombardment has been reported in several cathode wear tests and ion thruster life tests.

With sufficient gas flow, thermionic hollow cathodes can produce quiescent discharges at currents of amperes to many tens of amperes. However, as the discharge current is increased for a given cathode orifice size and gas flow rate, the noise observed in the discharge voltage and probe signals from the plasma increases, and the cathode produces ions with energies significantly in excess of the discharge voltage.[2–6] Cathode orifice plate and keeper electrode erosion rates measured or inferred in various experiments[7–9] and in ion thruster life tests[10–12] on the NASA Solar electric propulsion Technology Applications Readiness (NSTAR) ion thruster[13] have been found to be much higher than anticipated given the low voltages (typically <30 V) applied to the discharge. These results have been attributed to the high-energy ions bombarding and sputtering the cathode electrodes. Models proposed to explain the production of these energetic ions utilize a dc potential hill[14] located inside or just downstream of the cathode orifice, or ion acoustic instabilities in a double layer postulated in the orifice of the cathode.[2] However, there have been no direct measurements of potential hills or unstable double layers at the cathode orifice or in the cathode plume in probe studies to date[15–17] that might explain the mechanisms responsible for the high-energy ions or the electrode wear rates and patterns.

To investigate this issue, two different size hollow cathodes were installed in a test facility[15] at the Jet Propulsion Laboratory (JPL) that was instrumented with an array of scanning probes and a 4-grid retarding potential ion energy analyzer (RPA). The probes are very small (0.5 mm diam ceramic tubes) to avoid perturbing the plasma, and are scanned pneumatically at speeds of up to 2 m/s to avoid melting the probe tips in the high-density plasmas found in the near-cathode and keeper regions. The cathodes used in these experiments were a standard "1/4" NSTAR ion thruster discharge cathode,[13] which will be called the 0.635 cm cathode, and a larger, 1.5 cm diam hollow cathode from the Nuclear Electric Xenon Ion System (NEXIS) ion thruster.[18] The cathodes were installed in a conical-to-cylindrical anode arrangement that approximates the 30 cm
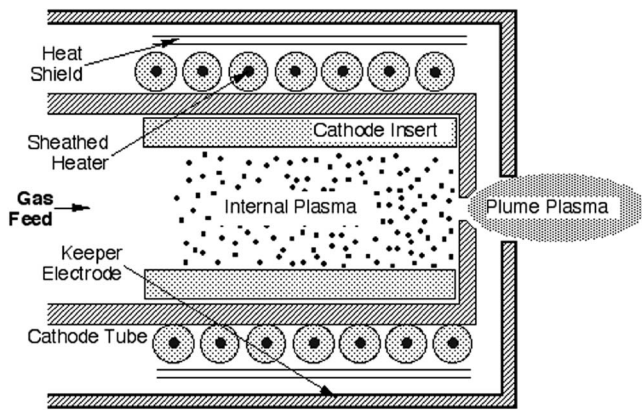
a)Electronic mail: dan.m.goebel@jpl.nasa.gov

14, 103508-1

FIG. 1. Generic hollow cathode configuration with internal insert, sheathed heater and keeper electrode.

FIG. 2. Schematic drawing of the experimental layout showing the cathode, anode, three scanning probe diagnostics, and the retarding-potential analyzer (RPA) which could be located radially or axially from the cathode.

diam NSTAR ion thruster anode geometry[13] and operated at various discharge currents and gas flow rates associated with different power levels or "throttle levels" of the thruster discharge.

The experiments detected relatively few ions with energies higher than the discharge voltage flowing downstream from the cathode on axis, but found a significant number of high-energy ions traveling in the radial direction from the characteristic "plasma ball" observed in front of the cathode for some discharge conditions. A detailed investigation of the dc and rf plasma density and potential profiles measured throughout the hollow cathode discharge by the scanning probes indicates that there is no dc potential hill at or near the cathode orifice. Measurements of the plasma potential fluctuations with an emissive probe constructed to be sensitive to up to 1 MHz show large amplitude fluctuations (>50 V) in the plasma potential ranging from 50 to over 200 kHz starting at the edge of the ball and extending radially outward to the wall. Measurements of the ion density fluctuations by the probes connected to a high-speed oscilloscope show moderate amplitude incoherent oscillations at frequencies up to about 2 MHz. The collected current by the RPA is correlated to the density and potential fluctuations measured by the probes. The potential fluctuations can exceed five times T_e, suggesting that turbulent acoustic oscillations and/or ionization instabilities exist under certain conditions near the cathode/keeper exit. Ions generated in this region at the peak of the plasma potential fluctuations acquire a large energy as they leave the plasma and strike the cathode electrodes and anode wall, which causes the significant sputtering of the surfaces near the cathode plume. The variation in the magnitude of the potential fluctuations and the change in the characteristics and location of the unstable region of the plasma ball as the discharge parameters and geometry change likely explain the different erosion rates and locations observed in different experiments.

In this paper, the experimental arrangement is described in Sec. II, and the presence of energetic ions measured by the RPA for these two cathodes shown in Sec. III. The plasma parameters and profiles measured throughout the hollow cathode discharge are presented in Sec. IV, and a characterization of the different fluctuations and their dependence is
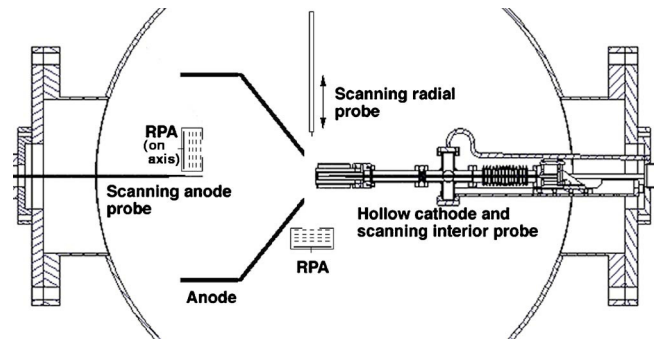
given in Sec. V. A brief discussion of the suppression of the observed fluctuations and a reduction in the energetic ion production is given in Sec. VI, and a conclusion is provided in Sec. VII.

II. EXPERIMENTAL ARRANGEMENT

The JPL cathode test facility[15] with the scanning probes and RPA is shown schematically in Fig. 2. The first cathode investigated in this facility is a conventional NSTAR-size hollow cathode[13] with a 0.635 cm outside-diameter molybdenum-rhenium tube with a 1 mm diam orifice. A porous tungsten emitter impregnated with a low-work-function barium-calcium-aluminate mixture is located inside this cathode, as illustrated in Fig. 1. Electrons emitted from the insert by field-enhanced thermionic emission generate a cathode-plasma inside the insert region from which electrons are extracted through the orifice to generate the plasma in the discharge chamber. The cathode is initially heated to electron emission temperatures by a sheathed heater coiled around the tube, which is turned off once the normal discharge is started. A keeper electrode made from molybdenum or graphite fully encloses the cathode, and the keeper orifice is about 4.8 mm in diameter. The second cathode has a conventional barium impregnated tungsten insert in a 1.5 cm diam molybdenum tube with a 2.5 mm diam orifice in the tungsten plate e-beam welded on the end. This cathode is also heated by a standard sheathed heater, which is turned off during discharge operation. The 1.5 cm cathode has a graphite keeper electrode that fully encloses the cathode, and the keeper orifice is the same size as the used in the 0.635 cm cathode.

The cathode is mounted on a Conflat flange installed in one port of the 0.75 m diam, 2 m long vacuum chamber. The chamber is pumped by two 10 in. CTI cryopumps with a combined xenon pumping speed of 1275 l/s for xenon. The base pressure of the chamber is 1×10^{-8} Torr, and during normal operation about 5 sccm of xenon flow the chamber pressure remains in the low 10^{-5} Torr range, where the xenon gas is controlled and measured by a calibrated digital mass flow controller. Additionally, a precision Baratron capacitive manometer is used to measure the pressure in the hollow cathode during operation, data from which has been reported elsewhere.[15,16]

The experimental arrangement uses a water-cooled anode that has a conical section transitioning to a cylindrical section approximately 30 cm in diameter with a NSTAR-like "ring-cusp" magnetic field arrangement. A solenoid coil positioned around the cathode produces an axial magnetic field at the cathode orifice, which couples to two rings of permanent magnets around the anode body to simulate the NSTAR magnetic field geometry. This anode geometry is capable of producing stable discharges from 5 A to over 50 A at discharge voltages of 20–40 V. In these experiments, the 0.635 cm cathode was run primarily at 8.2 A at 26 V and 13.1 A at 25.5 V, representing the two conditions in the NSTAR thruster (throttle levels TH08 and TH15, respectively) at which significant data on the erosion of the keeper electrode by high energy ion bombardment has been reported. The 1.5 cm cathode was run primarily at 25 A and about 26 V, corresponding to the nominal operating point of the NEXIS ion thruster, and was also run at several operating points above and below this level for comparison purposes.

The scanning probe used to measure the plasma parameters and oscillations inside the hollow cathode in the insert region has a 0.5 mm diameter alumina tube with a 0.127 mm diam tungsten wire electrode that protrudes from the single-bore ceramic tubing a distance of 0.25 mm. Even though the wire electrode length has been minimized, the probe has collected over 5 A of electron current during voltage sweeps in the high-density region inside the cathode near the orifice plate. The cathode probe is aligned axially in the system by two slide-guides internal to the cathode system. The probe has a linear throw of 4 cm and can traverse the cathode at 1–2 m/s, which produces a residence time of about 10 ms in the orifice region and a position resolution of 0.25 mm. A dual bellows system in the cathode assembly is used to keep a constant volume inside the cathode assembly, which maintains a constant pressure in the cathode while the Langmuir probe is being inserted into and out of the insert region. With the 0.635 cm cathode installed, the cathode probe occupies about 25% of the cathode orifice cross-sectional area, and significantly perturbs the plasma discharge (>5% change in discharge voltage or current) if the probe is pushed too far past the upstream orifice entrance. For this reason, data are collected prior to the probe entering the cathode orifice. With the larger 1.5 cm cathode, inserting the probe into the orifice does not significantly perturb the discharge (≤1% change in discharge voltage and current), and plasma parameters in the cathode orifice and keeper region can be measured.

The scanning-probe assembly used in the anode region also uses a pneumatic plunger and vacuum bellows arrangement mounted on the outside of the vacuum system. The diameter of the ceramic tubing interior to the vacuum system is stepped down from 3 mm to 0.5 mm for the 3 cm long section that is inserted deepest into the plasma in order to minimize perturbation to the plasma in the anode region. The exposed electrode is usually a 0.25 mm diam tungsten wire, with a length of 1.3 mm to collect sufficient current away from the keeper region to accurately determine the plasma parameters. The anode probe has nearly three times the throw of the cathode probe and five times the unsupported length so as to not perturb the anode-plasma, and also moves
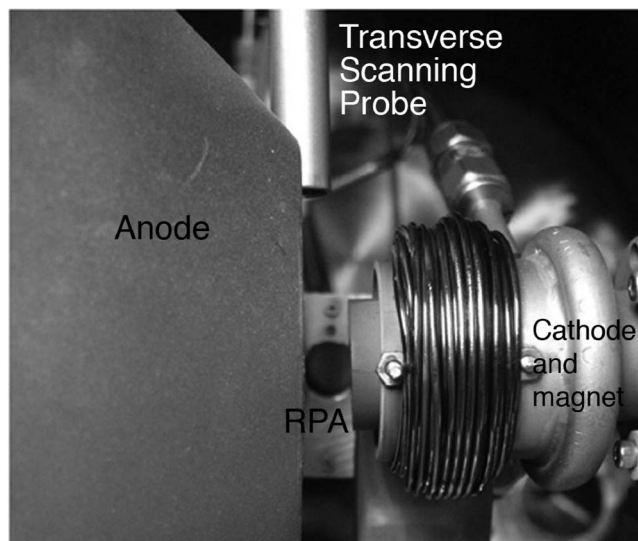

FIG. 3. Photograph of the 0.635 cm cathode, conical anode, RPA in the background, and transverse probe housing coming in from the top.

at 1 m/s with a position resolution of 0.5 mm. Very careful iterative alignment techniques are used to ensure that the anode probe is aligned with the cathode orifice and within 0.5 mm of the centerline. The anode probe can be fully inserted into the keeper orifice, although whip of the long ceramic sometimes causes the tip to touch the keeper or cathode during retraction.

The radially scanning emissive probe uses a pneumatic plunger mounted external to the vacuum system, identical to the cathode plunger arrangement, and is mounted to an X-Y manipulator outside the vacuum system to provide positioning relative to the keeper exit point. The radial probe has a linear throw of 4 cm with a speed of about 1 m/s, and is aligned by a slide-guide internal to the vacuum system to obtain a position resolution of 0.25 mm. The probe can be positioned in front of the keeper as close as 1 mm from the face to 2.5 cm downstream. The probe tip is a 0.127 mm diam tungsten hairpin wire fed through two side-by-side 0.5 mm diam alumina tubes. A floating 5 A power supply provides the current to heat the tungsten wire electrode to emit electrons. The probe is normally operated in the floating-mode[19] where the filament is heated sufficiently to saturate the measured potential found at the highest density. The plasma potential signal is fed to a high-impedance, high frequency circuit and buffer amplifier to detect any oscillations present in the signal. When the emissive probe is not in use, it is pulled back into a 6.5 mm diam tube that is positioned sufficiently out of the discharge plume to protect it from ion bombardment.

A gridded RPA is used to determine the ion energy distribution. A four-grid arrangement is used where the first grid in contact with the plasma is allowed to float, the second grid is biased to repel electrons, and only the ions with energy greater than potential applied to the dual-discriminator third and fourth grids can pass through and reach the collector. A photograph of the RPA positioned radially from the gap between the anode and the keeper is shown in Fig. 3. The gap

between the cathode keeper exit and anode is adjustable, and is typically about 1 cm to allow for visualization of the cathode plume and to acquire radial RPA data. The RPA can also be moved on axis to obtain axial energy distributions downstream from the cathode. In this case, the anode probe assembly is removed from the chamber to allow the RPA to be placed unobstructed on axis at the exit of the anode.

The bias voltage applied to the probe tips is generated by a programmable waveform synthesizer that drives a bipolar power supply. The voltage waveform is typically a sawtooth ramp that scans from −10 to +50 V in the anode region and from −10 to +20 V in the cathode region, both over a time of 1 ms. When using the 0.635 cm cathode, the cathode probe can only be swept once per insertion to avoid overheating the probe tip in the very high-density plasma ($>10^{15}$ cm^{-3} density) near the hollow cathode orifice. The 1.5 cm cathode has nearly an order of magnitude lower pressure inside and corresponding lower plasma density,[15] so that multiple voltage sweeps can be made during the probe insertion to map-out the plasma profiles with a single scan. Electron temperatures and plasma potentials are determined in less than half of the total 1 ms trace, therefore the position uncertainty for the plasma parameters is on the order of 0.5 mm over most of the scan and less than 0.25 mm near the full insertion point. The probe position, voltage and current data is collected on a PC at a sample rate of 300 kHz, resulting in 300 data points in each probe characteristic curve. Analysis of the plasma parameters from the probe data has been described elsewhere,[15] and follows the techniques described by Chen.[20] The probes are sized to always operate in the collisionless "thin-sheath" regime[20] where the probe radius is typically more than the ten times the Debye length due to the high plasma densities inside and within several centimeters of the cathode exit, and the collision mean free path is much larger that the sheath size. The electron temperature is found by fitting an exponential curve to the electron retardation region of the Langmuir trace. The electron temperature error bars of about 0.5 V and the plasma potentials have error bars of ±1 V in the cathode region and up to ±2 V in the anode region.

III. HIGH ENERGY ION PRODUCTION

A significant amount of data on erosion of the cathode keeper by energetic ions has been published for the NSTAR ion thruster wear tests and life tests.[10,11,21] Figure 4 shows a cross section of the keeper electrode after the 8200 h Life Demonstration Test (LDT) (Ref. 10) at JPL. In this test, the NSTAR thruster was operated at the highest power level, TH15, corresponding to 2.3 kW of total thruster power and a discharge current of about 13 A at 25 V. The keeper in this test was connected to the anode through a 1 kΩ resistor, and self-biased 3–4 V positive relative to the cathode during normal operation. The molybdenum keeper downstream face was significantly eroded during the test, indicating significant ion bombardment of the surface. This keeper face erosion was identified after the LDT as a significant life risk for the thruster, and observations of the keeper electrode condition during the 30 000 h Extended Life Test (ELT) (Ref. 11)
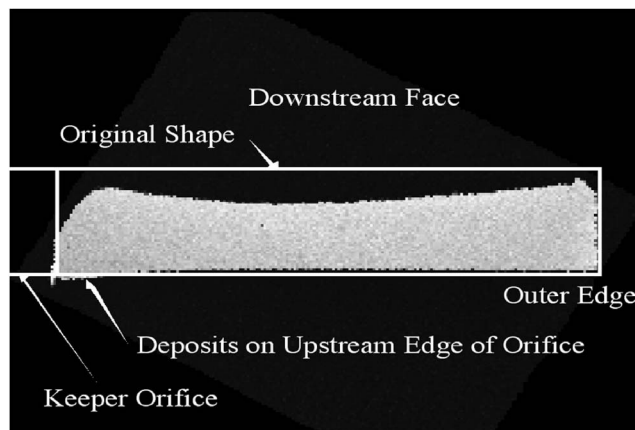

FIG. 4. NSTAR keeper cross section (from Ref. 10) after the 8200 h LDT test at TH15 showing significant erosion of the keeper face.

showed that the keeper surface eroded significantly and the keeper orifice diameter increased with time until the entire keeper orifice plate had eroded away. Without the keeper electrode, the cathode orifice plate and sheathed heater were significantly eroded during the thruster operation.

To understand the source of ions with sufficient energy to cause this erosion, the RPA was placed both on axis and radially in the gap between the keeper and the anode to diagnose the ion energy distributions. The axial measurements were taken with the RPA placed 25 cm downstream of the cathode exit, while the radial measurements were taken with the RPA positioned directly in front of the keeper electrode, as shown in Fig. 3, and 7.5 cm radially away from the discharge axis. The RPA discriminator grid was swept at a frequency of 10 Hz during these experiments, so the data shown in this section represents the time-averaged dc ion energy distribution. The ion energy distributions measured for the 0.635 cm cathode in the axial and radial directions from the RPA are shown in Fig. 5(a) for the TH15 (full power) mode and Fig. 5(b) for the TH08 (half power) mode. For the TH15 case, the ion energy distribution in the axial direction has a peak at the discharge voltage, and a larger peak observed at a lower potential. Since the RPA can only collect ions falling from the plasma potential peak in the discharge chamber to the grounded analyzer, there are many ions born at this discharge condition on the downward slope between the axial potential peak and the RPA that fall into the analyzer. Significantly, there are few ions with energies in excess of 35 V measured on axis. This is consistent with measurements made elsewhere.[22,23] The ion distribution measured in the radial direction has a peak slightly above the anode voltage, corresponding to ions born off axis at a plasma potential a few volts above the anode voltage. The radial ion energy distribution shows there are a large number of ions with energies significantly higher than the discharge voltage and extending out beyond 100 V.

For the TH8 throttle point, the axially positioned RPA shows the typical peak at about the discharge voltage, and relatively few ions with energy in excess of 40 V. The axial ion energy is again a result of the ions coming from the potential at which they were created or downstream of the
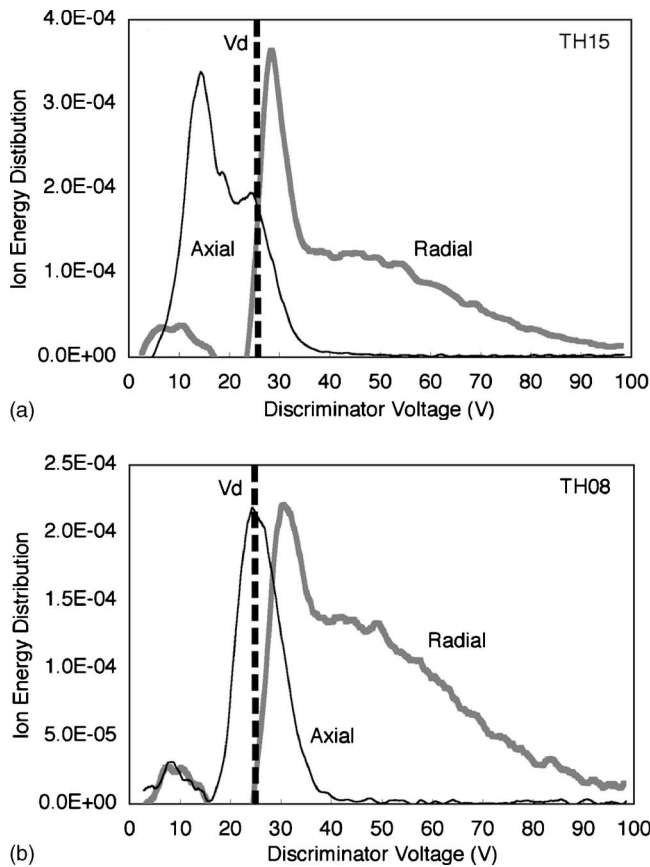
FIG. 5. Ion energy distributions radially (a) and axially (b) for the 0.635 cm diam cathode for two NSTAR throttle levels.
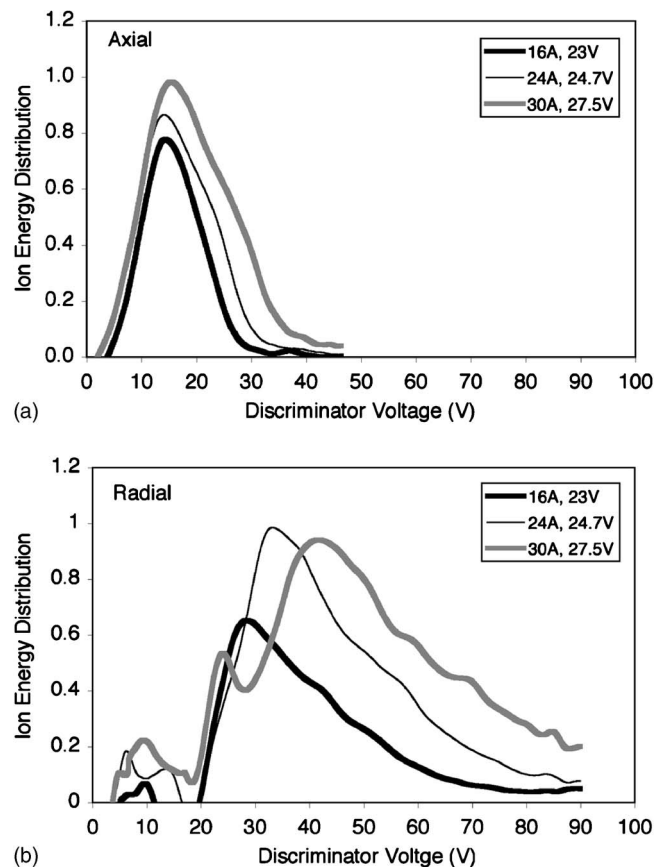

FIG. 6. Ion energy distributions radially (a) and axially (b) for the 1.5 cm cathode with a constant gas flow rate and three different discharge levels.

potential peak in the discharge chamber and falling into the cathode-potential analyzer. An analysis of the sputtering rate of the cathode and keeper orifices indicates that ions with over twice this energy would be required to produce the observed erosion rates in the ion thruster tests. The radial ion distribution, on the other hand, shows a significant number of ions at energies well above the peak magnitude near the anode voltage and extending out to 100 V, similar to the TH15 results.

Likewise for the 1.5 cm cathode, Fig. 6(a) shows the ion energy distribution from the RPA positioned directly on axis and positioned 25 cm downstream for various discharge currents at a constant xenon gas flow rate of 5.5 sccm through the cathode. The ion energy again is the result of the ions falling from the potential at which they were created into the cathode-potential analyzer. The axial data shows a broad distribution of ion energies from ions created at plasma potentials from several eV above the anode voltage down to several eV above the cathode potential. The maximum ion energy measured in this orientation increases slightly with discharge current to about 40 eV, which is consistent with the ion energies measured on axis in other experiments.[22]

Figure 6(b) shows the ion distribution functions for the same discharge cases as in (a) but measured with the RPA positioned immediately downstream of the cathode keeper exit and oriented radially from the cathode plume (as in Fig. 3). In this orientation, the RPA detects ions with energies starting just above the discharge voltage and extending to

values well in excess of 100 eV. Higher currents are observed to significantly increase the number of high-energy ions observed in the discharge. These ions are sufficiently energetic to cause the high keeper and cathode orifice erosion from sputtering reported in the literature. The high-energy ion tail found in the radial direction from the cathode plume is consistent with some measurements at other laboratories of higher energy ions detected in the downstream region of the thruster, but measured off-axis from the cathode.[3,23] This suggests that the energetic ion motion is not purely radial, but will have some axial component.

IV. PLASMA PARAMETERS IN THE DISCHARGE

To find the source of the high-energy ions, the complete axial and radial profiles of the plasma density, potential and electron temperature in the cathode insert, cathode plume and keeper regions were measured for both sizes of cathodes. These measurements include the time-averaged dc values of these parameters, and the high frequency characteristics of the plasma density and potential.

A. NSTAR cathode plasma data

The axial density, potential and electron temperature profiles measured from the hollow cathode insert-region plasma through the cathode orifice and into the anode-plasma region for the 0.635 cm diam NSTAR cathode are shown in Fig. 7. The plasma potential measured inside the
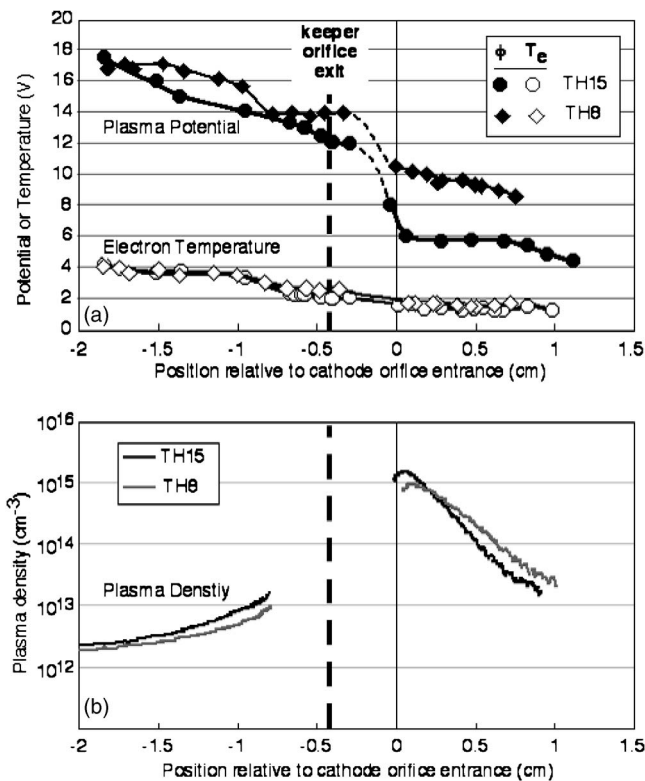
FIG. 7. Axial plasma potential and electron temperature (a), and plasma density (b) profiles for the 0.635 cm cathode for the TH15 and TH8 throttle levels.

FIG. 8. Radial plasma density 3 mm downstream of the 0.635 cm cathode keeper for the TH15 and TH08 throttle levels.

cathode in Fig. 7(a) for the 13.1 A TH15 mode at a discharge voltage of about 25 V is about 6 V, while a higher potential of 8–9 V is required for the 8.2 A TH8 mode to self-heat the cathode. The electron temperature in both cases is on the order of 1.5 V, and does not vary significantly as the cathode current is changed due to the high pressure inside the insert region. The potential in the region between the cathode and the keeper is difficult for the cathode-probe to measure because the diameter of the probe's ceramic tube is half the cathode orifice diameter, and the discharge is significantly perturbed by inserting the cathode probe deep into the orifice. However, inserting the anode-probe from the downstream side can penetrate inside the keeper orifice within a couple of millimeters of the cathode orifice without significantly altering the discharge. We see that the potential jumps to the order of 12–14 V for both discharge conditions, and then increases slowly as the probes moves away from the keeper orifice. The axial potential is found to reach about the anode potential within 5–10 cm of the cathode depending on the discharge conditions and local axial magnetic field profile.

The plasma density inside the 0.635 cm cathode is very high, as shown in Fig. 7(b), and is observed to exceed 10^{15} cm^{-3} for all but the lowest power discharge conditions. In changing operating conditions from TH8 to TH15, which increases both the discharge current and flow rate, the density profile is shifted downstream toward the orifice. The neutral pressure inside the cathode for TH15 is on the order of 8–9 Torr, and is about 1.7 times that of TH8. Higher
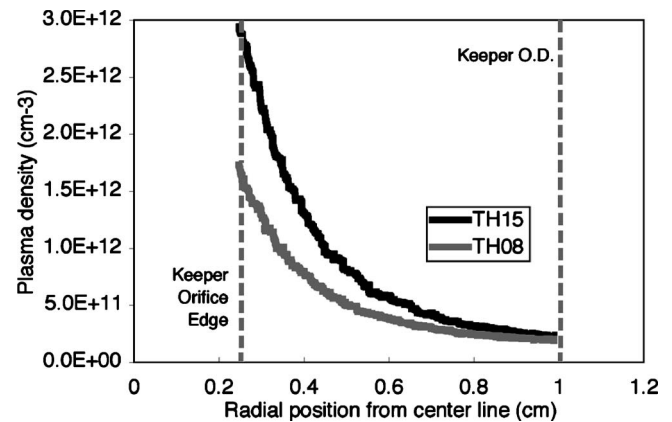
neutral pressures in the insert region are always observed to push the peak density location downstream and cause the cathode plasma density to fall more rapidly upstream from the orifice,[15,16] which reduces the already small contact area between the plasma and the emitting insert surface. The plasma is in contact with the insert typically less than about 3 mm for this cathode, suggesting that cathodes with pressures approaching 5–10 Torr may utilize only a fraction of the insert length for any significant electron emitting area.[15]

The plasma density downstream of the 0.635 cm cathode is observed in Fig. 7(b) to fall rapidly away from the keeper orifice in the axial direction, and also falls rapidly in the radial direction as seen in Fig. 8. In this case, the radially scanning probe is used to measure the local plasma density 3 mm downstream of the keeper face. While on-axis the plasma density at this axial location exceeds 10^{13} cm^{-3}, off axis the density falls to the order of 10^{12} cm^{-3} at the edge of the keeper orifice to less than 10^{11} cm^{-3} at the outside diameter of the keeper electrode. This large gradient occurs because the ≈ 100 G axial magnetic field applied in this region provides sufficient electron confinement to produce the strong radial density gradient.

The plasma density and potential profiles obtained farther downstream of the keeper electrode in the NSTAR thruster geometry have also been measured by Herman and Gallimore,[24] Sengupta *et al.*,[25] and Jameson *et al.*,[26] and their results are consistent with this data when our probes are configured to measure the time-averaged (essentially dc) plasma parameters. An example of the dc radial plasma potential profiles measured by our radially scanning emissive probe positioned about 3 mm downstream of the keeper for the two discharge cases is shown in Fig. 9. In this case, the data acquisition system utilized a low-pass filter that averaged the data at about 1 kHz, so this data represents the time-average radial potential profile. We see that the plasma potential is about 12 V on axis for the TH15 mode, in agreement with the anode Langmuir probe data in Fig. 7(a). The potential is a minimum on axis and increases to above the anode potential a distance of about 1 cm radially from the axis. Likewise, the lower current TH08 mode has a potential on axis of about 15 V, and increases rapidly in the radial dimension toward the anode. Similar profiles extend axially such that
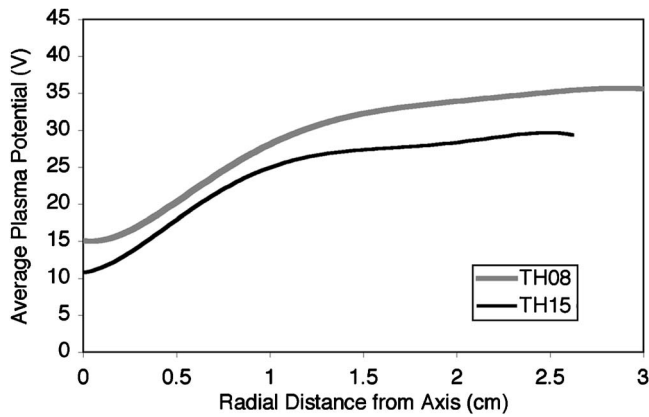
FIG. 9. Radial time-averaged plasma potential from the scanning emissive probe for the 0.635 cm cathode at TH15 and TH08.

FIG. 10. High frequency plasma potential oscillations for the 0.635 cm cathode at the TH15 and TH08.

the cathode plume forms a potential trough, with the potential increasing radially and axially from the keeper orifice exit. This spatial potential behavior is inverse to the plasma density profiles, which are peaked near the cathode exit and decrease radially and axially away from the keeper.

The plasma data indicates that the time-averaged plasma potential in the region immediately downstream of the cathode exit is actually the lowest found in the entire discharge chamber. The plasma density decreases monotonically from the keeper exit both axially and radially, and electron temperature is relatively flat. Primary electrons coming from the insert region through the potential step in the orifice have a relatively low energy (<15 V), and do not appear to drive any unusual density structures or potential peaks in the keeper or cathode orifice regions. The potential structure forms a trough leading back into the keeper orifice, and not the potential hill theorized to produce high-energy ions.[3] Singly charged ions born in the cathode plume region, from a dc potential sense, will tend to flow back towards the cathode and bombard the keeper and cathode orifice with very low energy (<20 V), which will not cause the erosion rates or patterns observed in other experiments.[27]

The source of the high-energy ions flowing in the radial direction for both throttle levels was investigated. Since the ions fall from the potential at which they are created, there is no mechanism for the observed high ion energies reported in the literature in the dc-averaged potential profiles we measure (Figs. 7 and 9) and that are found in the literature.[17,24,25] However, if the plasma potential near the cathode exit is oscillating, some fractions of the ions will be created at a higher potential and gain energy falling toward the keeper that may be sufficient to sputter the keeper at high rates. The rf oscillation of the plasma potential in the cathode plume was examined with the transverse emissive probe operated in the emission-limited mode[19] in which the probe filament is heated to a sufficient temperature to emit electrons at the random plasma electron flux (or higher), and the probe thereby floats close to the local plasma potential. A high impedance circuit ($>10^8$ Ω) capable of detecting up to 1 MHz oscillations was designed and used to measure the plasma potential fluctuation profile radially in front of the keeper face plate.
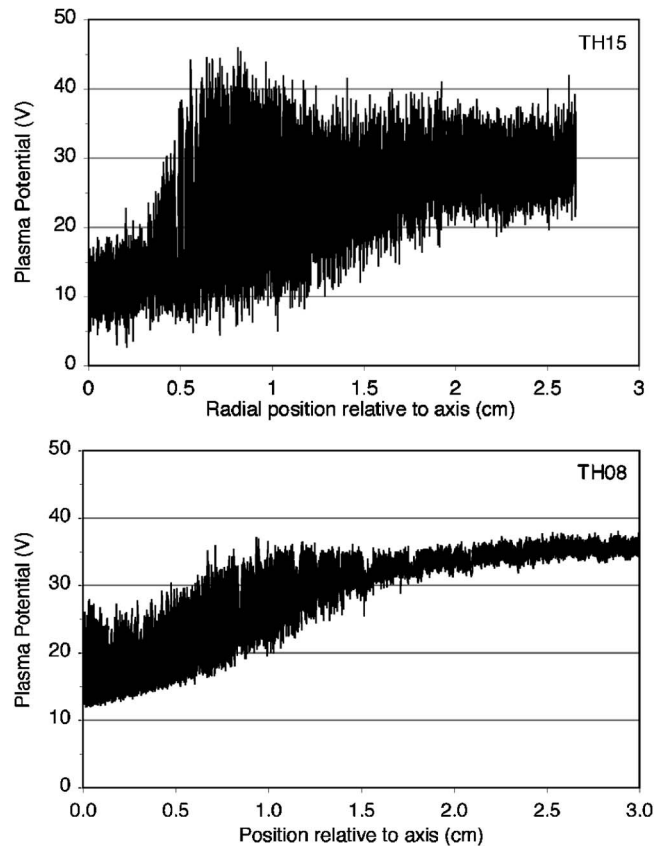
Figure 10 shows the radial profile of the plasma potential from the rf-emissive probe at a distance of 3 mm downstream of the keeper for the two discharge conditions. The data again shows that the average plasma potential has a minimum on axis at about 12 V, in agreement with the data-acquisition-averaged results in Fig. 9. As the emissive probe moves radially outward, the plasma potential increases significantly to above the discharge voltage all along the keeper face, and eventually decreases back to the anode potential near the anode wall (beyond this scan). The potential oscillations in the keeper region were found to be primarily between 50–500 kHz, depending on the specific operating conditions. Measurements of the oscillation frequency using a spectrum analyzer and standard floating-probes showed that the fluctuation amplitude decreased monotonically with frequency above several hundred kilohertz out to tens of MHz, which is characteristic of these types of discharges.

The plasma potential fluctuation level in the TH15 mode range from ±5 V at the axis to sometimes over ±20 V about 1 cm off axis, with the largest fluctuations starting at about 6 mm from the axis out to 10 mm. This results in peak rf plasma potentials off axis in excess of 40 V. In the TH08 mode, the magnitude of the fluctuations is smaller compared to the TH15 mode, and the maximum potential is lower. This behavior is always observed in that the higher the discharge current, the higher the plasma potential fluctuation level for a

given gas flow rate. Only when the gas flow rate is significantly increased can the fluctuation levels be decreased at higher discharge currents.

Since the fluctuation levels can exceed 5 times the local electron temperature and have a frequency of typically under 1 MHz, these oscillations are likely related to turbulent ion acoustic waves or ionization instabilities in the near-cathode plume region.[28] Instabilities of this type have been suggested as the mechanism for enhanced resistivity and nonclassical plasma transport in this region in recent modeling of hollow cathode plumes.[28] The high frequency fluctuations are observed to be relatively incoherent (their frequency changes randomly) and are observed all along the radial scan, but are found to decrease in amplitude as the probe is moved axially farther downstream in the cathode plume. The maximum amplitude of the rf oscillations in the plasma potential is always found in the "plasma-ball" region observed immediately downstream and within about 1 cm of the keeper exit.

B. NEXIS cathode plasma data

To examine the scaling of this discharge behavior with cathode size and provide a more detailed study of the plasma parameters in the cathode orifices and the oscillation characteristics, a larger NEXIS 1.5 cm diam thermionic hollow cathode with a 0.25 cm diam cathode-orifice was installed in the system. The magnetic field configuration was identical to the 0.635 diam cathode case, except that the axial field at the cathode orifice was reduced to 78 G consistent with the NEXIS ion thruster design.[18,29] Figure 11 shows axial plasma potential, electron temperature and density profiles measured throughout the system at the nominal 25 A of discharge current and 5.5 sccm xenon cathode-gas flow. At the standard 1 kHz voltage sweep rate used for the Langmuir probes in these experiments and the 1 m/s probe-scanning speed, the data points in Fig. 11 have a position resolution of about 0.05 cm. While the data acquisition system samples at a rate of up to 500 kHz/channel, the frequency response of the Langmuir probe circuits is only about 50 kHz. Therefore, these measurements represent time-averaged dc values.

Inside the hollow cathode, the plasma potential for the nominal discharge conditions is about 12 V above the cathode potential, consistent with the desire to obtain a reduction in the ion energy bombarding the low work-function electron-emitting surface and preserve the low work function barium-oxide surface. Inside the cathode orifice, the plasma potential increases by about 10 V, and the plasma potential is essentially flat through the 0.5 cm long keeper region. The plasma potential then increases slowly downstream of the "plasma-ball" region to a peak of about 30 V (about 5 V above the anode potential) several centimeters downstream of the cathode. The electron temperature is observed to be 2–3 eV inside the cathode, increasing up to 5 eV in the downstream cathode plume and remaining relatively flat throughout the downstream anode region plasma.

The plasma density inside the hollow cathode is in the low 10^{14} cm^{-3} range, and falls from there to nominally around 10^{13} cm^{-3} in the keeper region and below 10^{12} cm^{-3} in the anode region, consistent with the plasma density de-
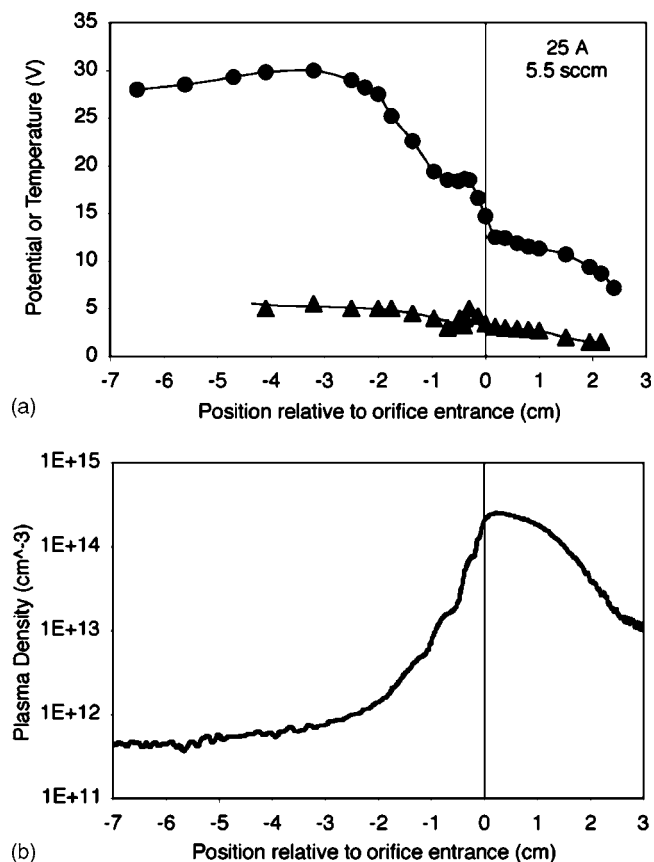

FIG. 11. Axial plasma potential and temperature (a) and density (b) profiles for the 1.5 cm cathode operating at 25 A of discharge current.

sired near the grids for ion thruster operation. The axial density and potential profiles are observed to change monotonically from the cathode orifice region into the anode region, which was not able to be directly measured in between the cathode and keeper orifices in the smaller 0.635 cm cathode. The larger cathode orifice size permits inserting the probes well into the cathode and keeper orifices without perturbing the plasma discharge more than about 1% in voltage and current, providing complete profile data through this critical region. The transverse plasma density profiles for different axial positions from the keeper exit for this larger cathode are also shown in Fig. 12. As with the 0.635 cm cathode, the plasma density is the highest on axis and near the cathode, and the cathode plume disperses radially as the axial distance from the keeper increases.

The time-averaged (≤ 1 kHz) radial profile of the plasma potential 3 mm downstream of this cathode at 25 A with two different gas flow rates is shown in Fig. 13. The potential on axis is found to be less than 20 V, consistent with the Langmuir probe data shown in Fig. 11. The potential increases from the axis radially toward the anode, forming a radial potential well and axial potential trough consistent with that observed with the 0.635 cm cathode. As the gas flow is decreased, the average potential increases outside the cathode, but not sufficiently to explain the presence of 100 V ions that were described in Sec. III.

As with the 0.635 cm cathode, there is clearly no dc potential hill at or near the cathode keeper or orifice exit that
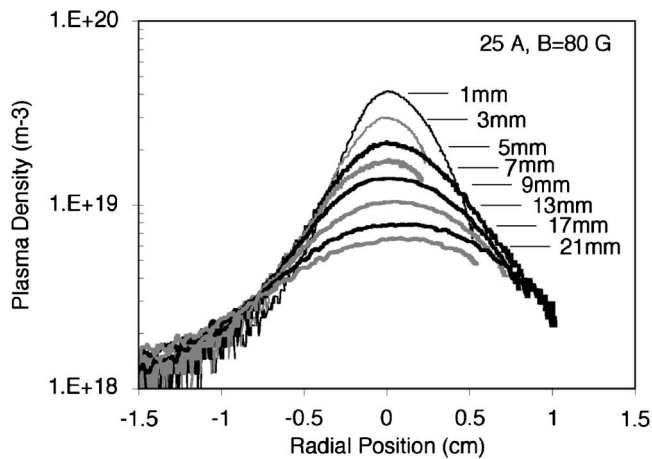
FIG. 12. Radial plasma density profiles for different distances from the keeper exit for the 1.5 cm cathode operating at 25 A of discharge current.

could produce the energetic ions observed by the RPA. The axial RPA data are consistent with ions generated downstream of the gradual potential peak that exists several cm downstream of the cathode and fall into the analyzer, while the radial RPA data cannot be explained by these dc potential profiles.

However, the rf plasma potential near the cathode exit can be extremely high, and the high frequency rf oscillations measured by the scanning emissive probe for the 0.635 cm cathode were also detected as with the 1.5 cm cathode. The transverse scanning probe was again configured as an emissive probe that is operated sufficiently hot to float at the plasma potential[19] and scanned directly across the keep face 2 mm downstream from the keeper. Figure 14 shows the radial plasma potential measured for the nominal 25 A, 25.5 V, 78 G case for two gas flow rates. For the nominal 5.5 sccm cathode flow, the rf plasma potential shown in Fig. 14(a) has fluctuations levels typically less than ±15 V and peak amplitudes near the keeper of less than 35 V. However, as the gas flow is reduced to 4 sccm in Fig. 14(b), the fluctuation amplitude increases dramatically with peak values exceeding 60 V.
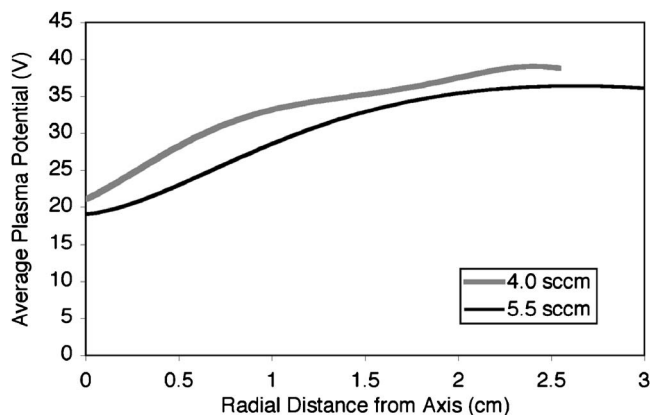

FIG. 13. Time averaged radial profile of plasma potential for the 1.5 cm cathode for two gas flows at 25 A and 78 G applied axial field.
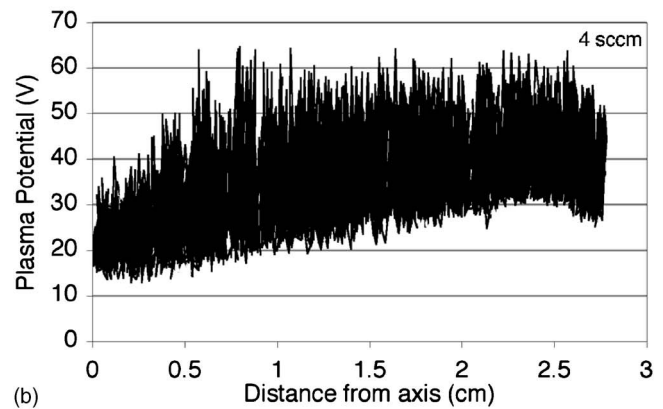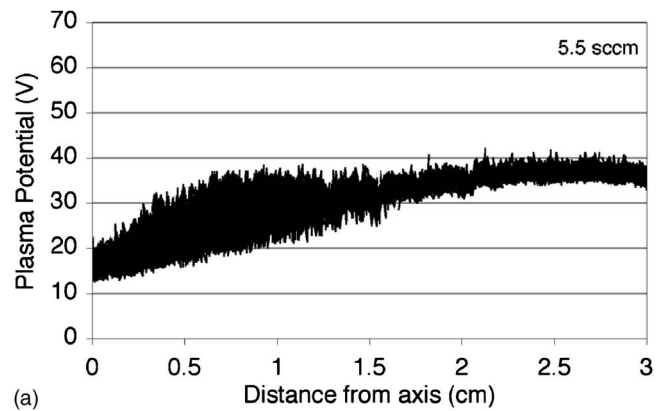

FIG. 14. High frequency plasma potential oscillations for the 1.5 cm cathode at 25 A for 5.5 sccm (a) and 4 sccm (b).

The amplitude and frequency structure of the potential and density fluctuations in the 1.5 cm cathode discharge were investigated in more detail. Figure 15 shows the plasma potential measured with the emissive probe at the edge of the plasma ball for the nominal case of 25 A, 5.5 sccm, and 78 G at the cathode exit (a), and for the case of no applied field at the cathode exit (b). These data were recorded on a 1 Giga-sample per second digital oscilloscope so that the actual frequencies up to the full bandwidth of the emissive probe detection circuit could be observed. As the applied magnetic field is reduced, increasingly higher amplitude potential oscillations, approaching a peak potential of 70 V, are observed. This same behavior is observed as the gas flow rate is reduced at a fixed magnetic field, which will be shown later. The nominal case in Fig. 15(a) has incoherent plasma potential fluctuations in the range of 200 kHz–1 MHz (the maximum frequency sensitivity of the probe-circuit) with an amplitude of less than 10 V. If the magnetic field is reduced, the fluctuation amplitude is observed to increase to about 50 V. The frequency of these oscillations is about 80 kHz, and they are characterized by being nonsinusoidal with varying amplitudes with time. These large-amplitude oscillations occur on ion-acoustic time scales, and will be shown later to likely result from local ionization instabilities.

The density fluctuations in the near-cathode plume region are significant even in the nominal case of Fig. 15(a) where the potential fluctuations are relatively small. Figure 16(a) shows the fluctuations in the ion saturation current (on
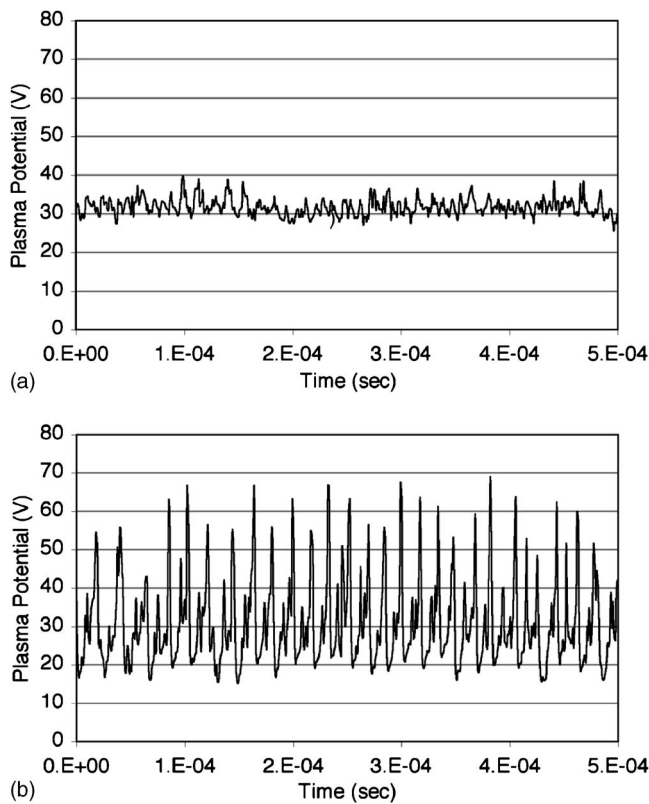
FIG. 15. Plasma potential oscillations measured at the edge of plasma ball for 25 A for 80 Gauss (a) and 10 Gauss (b) showing the onset of high amplitude ionization instabilities.

a faster time scale than Fig. 15) measured by the transversely scanning probe inserted into the edge of the plasma ball for the nominal 25 A, 5.5 sccm case. The oscillations are relatively incoherent with frequencies of 0.5–2 MHz and amplitudes approaching 100% of the ion saturation current. Re-
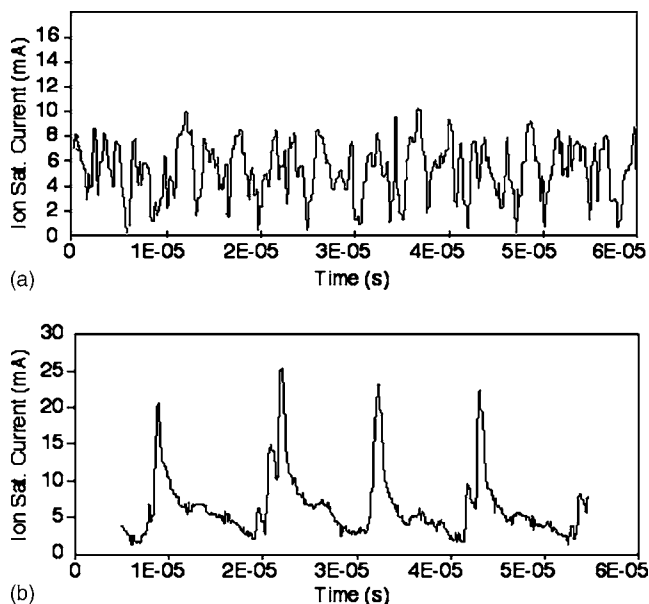

FIG. 16. Ion saturation current oscillations at the edge of the plasma ball for 25 A at 5.5 sccm (a) and 4 sccm (b). Note the time scale is different than in Fig. 15 so the characteristics of oscillations can be seen.
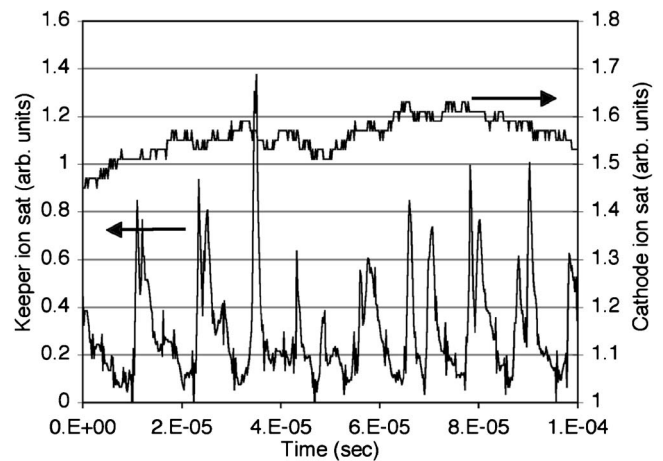

FIG. 17. Ion saturation current measured inside and outside the cathode showing no correlation to the oscillations in the hollow cathode insert plasma.

ducing the gas flow rate, as shown in Fig. 15(b), causes the oscillations to change into the lower frequency ($\approx$100 kHz) oscillations with large-amplitude fluctuations. The characteristics of these types of oscillations will be discussed in the next section.

V. CHARACTERISTICS OF THE FLUCTUATIONS

A. Inside the cathode

It has been proposed[2] that plasma instabilities in a double layer inside the cathode orifice can couple to the region outside the cathode and accelerate ions to high energy. Recent theoretical modeling[30,31] of the plasma region inside the cathode suggested that turbulence near the orifice entrance may develop as a result of wave growth from streaming electrons and ions, which are subject to reduced Landau damping due to the relatively low ion-to-electron temperature ratio ($\sim$0.1). However, these calculations only extended up to the orifice entrance where turbulent heating of the ions and electrons is likely due to the increasing electron current densities entering the orifice. To investigate proposed density oscillations in the cathode interior or orifice region, the scanning probes were biased to ion saturation and connected to the 1 Gbs digital oscilloscope. Figure 17 shows the ion saturation current data measured simultaneously by the transverse scanning probe in the plasma ball outside of the cathode and by the axially scanning probe located just upstream of the 1.5 cm cathode orifice plate for the zero applied cathode-magnetic-field case at the nominal discharge current and gas flow. The oscillations are not correlated or related in any way. Inside the cathode, and even inside the cathode orifice, low frequency ion-acoustic type oscillations with frequencies on the order of 1 MHz were detected, but were found to be small in amplitude ($\delta n/n \ll 10\%$). There were no significant oscillations detected inside the hollow cathode or in the cathode orifice region for the 1.5 cm cathode discharge. It is clear that the potential and density oscillations described above are generated in the cathode keeper and
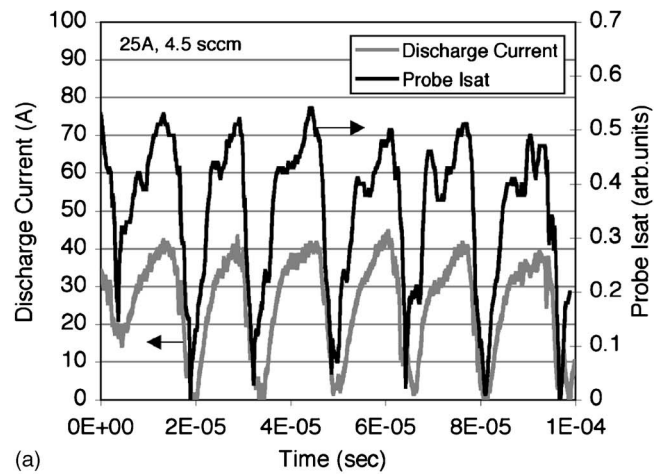
near-cathode plume region outside the cathode where $\delta n/n$ can exceed 1 and the oscillations propagate well into the anode-plasma region.

Previous descriptions of measurements of the NSTAR cathode plasma parameters[26] showed large density oscillations inside the discharge hollow cathode for the TH08 mode. However, a careful investigation of this case showed the presence of very large density and potential oscillations generated in the plasma ball region outside the cathode, similar to those shown in Fig. 10, that can trigger discharge power supply regulation oscillations.[32] These ≤1 kHz discharge supply oscillations then modulate the discharge voltage and current, which appears in the plasma density both inside the cathode and in the anode region. It appears that the TH08 mode in the NSTAR cathode is susceptible to breaking into even larger amplitude oscillations than shown here, which in this case triggered the discharge supply oscillation and large density changes in the hollow cathode. However, in all cases with the 1.5 cm cathode, the plasma oscillations observed did not trigger the power supply regulation problem.
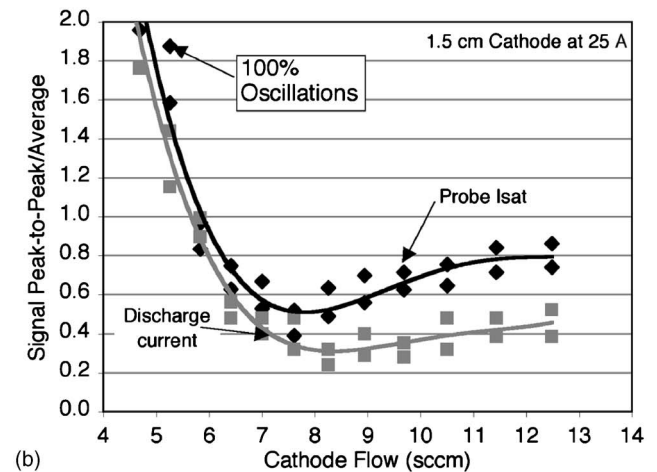
It appears that there are three classes of oscillation in these discharges: (1) high-frequency (0.1–2 MHz) turbulent ion acoustic oscillations of small to moderate amplitude, (2) medium-frequency (40–150 kHz) ionization instability oscillations that can have very large amplitudes, and (3) low-frequency (≤1 kHz) discharge power supply regulation oscillations. The high-frequency ion-acoustic oscillations are always present, and can be detected in the cathode orifice and keeper regions. The lower frequency oscillations occur in special cases of orifice size, discharge current, and cathode gas flow rate.

FIG. 18. Discharge current and ion saturation probe current downstream of the plasma ball (a), and peak-to-peak divided by the average probe and discharge current signals vs gas flow rate (b) for the 1.5 cm cathode. The minimum and maximum values of the oscillation level data is shown by the two points at each of the flow conditions.

B. Exterior to the cathode

The structure of the cathode plume and the appearance of the different types of oscillations discussed above are the result of different operating modes in the hollow cathode, but the transitions are gradual. While the medium-frequency (50–150 kHz) oscillations in the 1.5 cm cathode discharge did not trigger the very low frequency (≤1 kHz) power supply regulation oscillations, they could produce 100% modulation of both the discharge current and plasma density at low gas flow rates for a given current. Figure 18(a) shows the discharge current emitted from the hollow cathode and the ion saturation current to a probe positioned on-axis 3 cm downstream of the cathode for the case of 25 A, zero magnetic field, and 4.5 sccm of gas flow. The oscillations occur at the characteristic 80 kHz for this operating condition, and show that cathode emission current and plasma density oscillations in the cathode plume are strongly correlated. This behavior is characteristic of ionization instabilities where the plasma density is modulated on the ionization rate and neutral gas fill time constants. The rate of production of ions is given by

$$\frac{dn_i}{dt} = n_e n_o \langle \sigma v_e \rangle, \tag{1}$$

where n_i is the ion density, n_e is the electron density, and the term in the brackets is the ionization rate coefficient, which is averaged over the electron energy distribution function. The frequency of an ionization instability will then be approximately

$$f \approx \frac{d}{dt} = \frac{n_e \langle \sigma v_e \rangle}{(n_i/n_o)}, \tag{2}$$

where the denominator represents the local ionization fraction. These types of instabilities can grow for situations where the neutral and electron densities are of the same order if the electron temperature is sufficiently high to get significant ionization. In the region of the plasma ball 1 cm downstream of the cathode, the plasma density and electron temperature from Fig. 11 for the nominal discharge case for this cathode are 10^{13} cm^{-3} and 4 eV, respectively. At this temperature, the ionization rate coefficient for xenon is about 3.6×10^{-9} cm^3/s. For an ionization fraction of 40%, the ionization frequency is about 80 kHz, consistent with the fre-

quencies observed. Ionization fractions of 10%–50% in this region have been estimated using the 2D neutral and plasma codes[27] under development at JPL. The oscillation frequency of these instabilities in the 1.5 cm cathode discharge is also observed to increase with discharge current,[31] which is consistent with plasma density and temperature increasing in Eq. (2). Ionization instabilities in moderately high ionization fraction plasmas like these are sometimes called predator-prey oscillations[33] in that the ionization tends to deplete the local neutral gas, which causes the density to drop and reduce the discharge current-carrying plasma density. The system then oscillates on the ionization-rate time scales.

If the gas flow level or discharge current is changed, the amplitude of the potential and density oscillations are also observed to change due to variation in the ionization fraction and local plasma parameters. Figure 18(b) shows the peak-to-peak amplitude of the ion saturation probe signal divided by the average value (essentially $\delta n/n$) and the discharge current as the cathode gas flow is varied for a constant discharge current of 25 A. At each gas flow rate, the signal was stored and the minimum and maximum values of the oscillation level found for 10 samples of the signals are shown by the two points. Since the waveforms are not purely sinusoidal, the values can exceed 2 at low gas flows and represent 100% (on-off) oscillations in the discharge. As the gas flow is increased, the magnitude of the oscillations for both the probe signal and the discharge current decrease until a high-flow condition is reached and additional less coherent fluctuations emerge. Variations in the dc discharge current level for a given cathode orifice size shift this curve to the left and right, with higher current generating higher oscillation levels at any given flow rate. Similar behavior was observed for the 0.635 diam cathode but at different current and flow rates. The transition from the so-called quiescent "spot mode" to the noisy "plume mode"[34,35] is actually observed to occur continuously (not a sharp transition) as the gas flow decreases or the current increases. The transition of the oscillations from the high-frequency incoherent fluctuations to the low-frequency, larger-amplitude "predator-prey" oscillations was also achieved by reducing the applied magnetic field strength at the cathode exit, which affects the plasma production in this region in a similar manner as reducing the cathode gas flow. Since the plume mode is often defined as existing for a given discharge voltage oscillation level, significant fluctuations like these in the plasma itself are required to couple to the normally filtered voltage signals (due to capacitance in the power supplies) from the anode or keeper electrodes in order to detect the plume mode externally to the discharge.

C. Correlation of fluctuations to the energetic ions

The ion current collected by the RPA was compared to the plasma density and potential fluctuations measured by the probes. Figure 19 shows the Langmuir probe ion saturation current fluctuations measured at the edge of the plasma ball, the ion current collected by the RPA set at a discriminator voltage of 50 V to observe the energetic ions, and the ac component of the discharge voltage. While the ion current
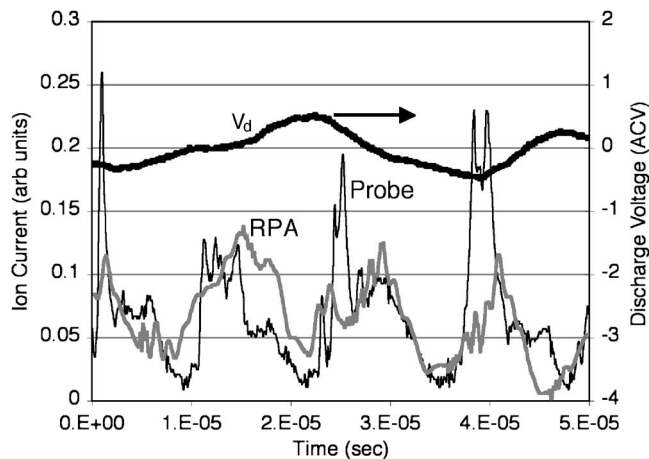

FIG. 19. Ion current from scanning probe positioned at the edge of the plasma ball, ion current collected by the RPA, and discharge voltage showing correlations between the energetic ions and the plasma fluctuations which are not power supply driven.

to the probe and the RPA ion current fluctuations are reasonably well correlated, these fluctuations are not driven by oscillations in the discharge voltage. The discharge voltage oscillations observed are typical of the normal low-frequency (≤ 1 kHz), small-amplitude ($< \pm 1$ V) power supply behavior as it regulates the discharge current.

For the nominal discharge condition with an applied magnetic field, the 1.5 cm cathode does not typically generate ionization instabilities, and the RPA current is only weakly correlated to the higher-frequency, turbulent plasma-potential fluctuations measured in the discharge by the probe. Figure 20(a) shows the high frequency plasma potential oscillations and the collected RPA current for the nominal discharge conditions of 25 A, 5.5 sccm, and 78 G applied magnetic field at the cathode exit. The amplitude of the oscillations on both signals is relatively small and poorly correlated, if at all. However, the low-frequency potential oscillations produced by a reduction in the applied magnetic field and shown in Fig. 20(b) are well correlated with the measured RPA ion current, but about 180° out of phase. This behavior is consistent with the ions being born at a high potential near the cathode and flowing to the RPA in bursts at the ionization oscillation frequency as the plasma density and potential collapse. If singly ionized xenon ions fall through 40 eV, they will arrive at the RPA located 7.5 cm away about 10 μs later, which is consistent with the time lag (phase shift) shown in Fig. 20(b).

A direct comparison of the ion energies for plasma conditions with and without the large amplitude oscillations was made using the radially positioned RPA for the two discharge cases in Fig. 20, and the results shown in Fig. 21. The zero magnetic field case (with the large oscillations) produces significantly larger numbers of high-energy ions compared to the nominal case. Since the probe currents and plasma potential measurements are related in magnitude and frequency to the energetic ion currents measured by the RPA, it is clear that the energetic ions are related to the plasma instabilities in the cathode plume. While there are mechanisms for accelerating the ions by ion acoustic waves, it is likely that a large
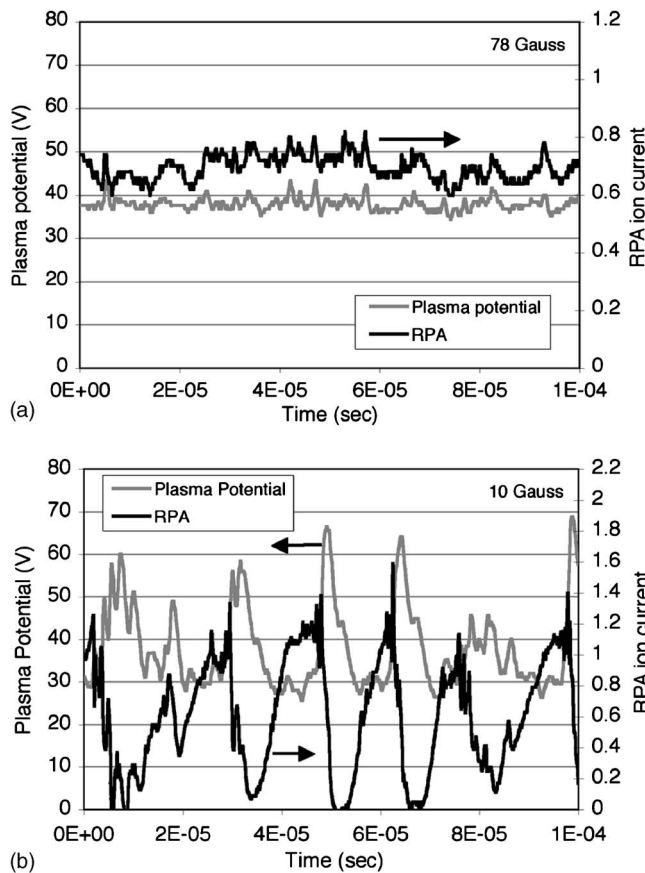
FIG. 20. RPA current and plasma potential oscillations for two cases of the applied magnetic fields at 25 A and 5.5 sccm.
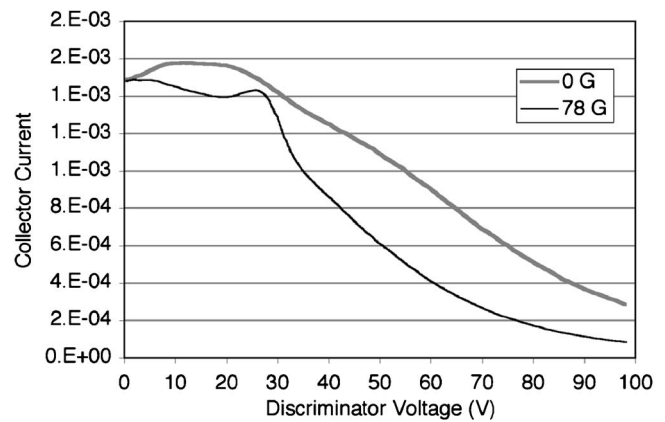

FIG. 21. Comparison of RPA current vs discriminator voltage for the case of zero magnetic field (with large amplitude oscillations), and nominal magnetic field (no ionization instabilities) for the 1.5 cm cathode.

fraction of the ion energy comes from ions being born at high potential during an oscillation in the plasma density and falling through that potential drop to the cathode potential RPA. Any doubly ionized xenon will also gain twice the energy by falling through the same potential, and will contribute to the higher energy ion tail. Recent measurements[36] indicate that the double ion content in the radial ion flux in front of the keeper can approach 10% of the ion current in some cases, which could contribute to the observed high-energy tail and the source of the observed erosion rates. However, calculations of the double ion production in the near cathode plume region of the NSTAR cathode in the TH08 and TH15 modes indicates that less than 1% of the ions generated locally are double ions, so that this does not appear to be the cause of the high erosion rates. Another possibility is that an ion energy multiplication mechanism based on charge-exchange collisions in the cathode plume[36] can contribute to the generation of the ion energies observed above the maximum potential fluctuation level. Theoretical and experimental investigations aimed at understanding the role of the instabilities and ion acoustic waves in producing the high-energy ions are still underway.[27,37]

Finally, the cathode plume structure and location of the plasma ball is observed to change with the discharge parameters. It is generally observed that increases in gas flow, discharge current, and magnetic field all push the plasma ball downstream. Increases in the gas flow generally reduce the

observed oscillation level, especially of the low frequency predator-prey modes associated with collapse of the plasma due to more complete ionization of the gas in the near-cathode plume. Figure 22 shows photographs of the cathode plume for the 1.5 cm cathode for the nominal 25 A, 5.5 sccm condition (a), and for a 12 sccm high flow rate case (b). The plasma ball moves significantly downstream at higher flow rates, and a dark space associated with very cold electron temperatures is observed to form between the cathode and the plasma ball. Probe measurements in the dark space region confirmed that the lowest electron temperatures found in the plume plasma (typically about 2 eV) exist in this region,[26] and the electron temperature increases to over 4 eV as the probe is moved downstream into the plasma ball. The electron temperature profile suggests that the plasma ball is a structure created in the plasma to enhance the ionization in the cathode plume sufficiently to carry the discharge current from the keeper region into the anode region. The proximity of the unstable plasma ball region to the keeper orifice may then influence the keeper erosion rate and patterns.

VI. FLUCTUATION AND ENERGETIC ION SUPPRESSION

It is clear from the data presented in Figs. 6 and 18(b) that there are operational scenarios in which the plasma fluctuations and related energetic ion production are reduced. The data show that higher gas flows and lower discharge currents for a given cathode geometry reduces the energy of the ions produced in the cathode plume. Likewise, larger orifices producing lower current densities and reduced ionization fractions in the near-cathode plume, in addition to proper selection of confining magnetic field strength, tend to reduce the oscillations and energetic ion production. This behavior is consistent with general design guidelines for hollow cathodes that have been passed down[38] that limit the current density in the cathode orifice to avoid operation in the plume mode.

Since the oscillations are related to either ionization instabilities or turbulent ion acoustic waves, both of which
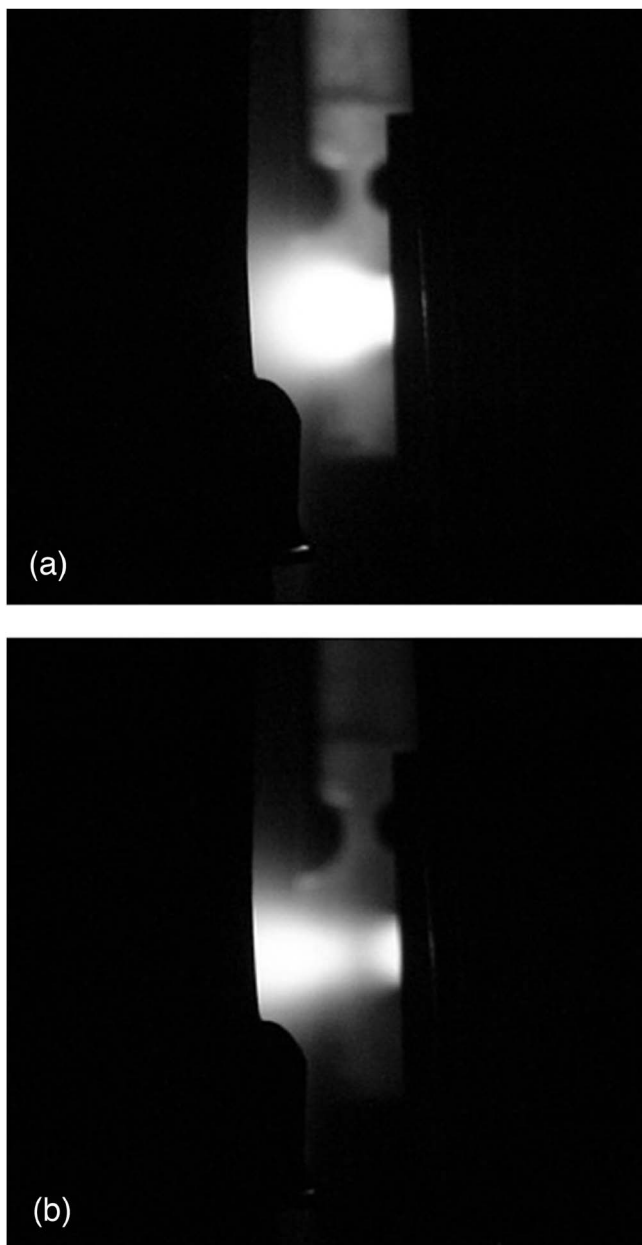
(a)

(b)

FIG. 22. Photo of the plasma ball region in front of the 1.5 cm cathode at 25 A with 5.5 sccm (a) and 12 sccm (b) gas flow rates through the cathode.
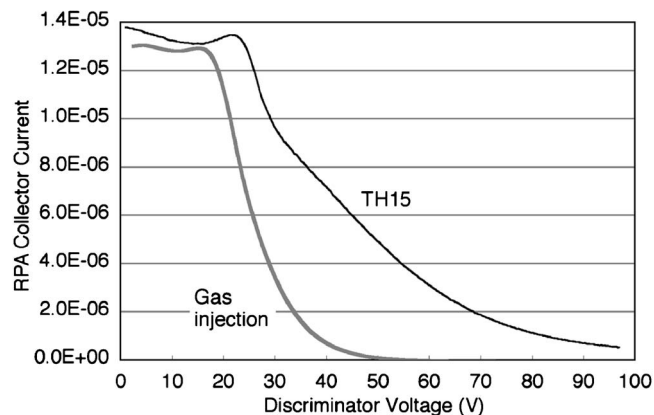

FIG. 23. RPA data for the 0.635 cm cathode at the TH15 discharge current level showing that gas injection into the cathode plume (the jet-mode) reduce the energetic ion production.

depend strongly on the local neutral gas pressure and plasma (electron and ion) temperatures, it is possible to damp the oscillations locally at the keeper exit. For example, a small gas-injection tube was positioned just downstream of the keeper orifice on the 0.635 cm cathode and about 1 cm off axis, and a small amount of xenon was injected directly into the plasma ball region.[38] This modification significantly dropped the impedance of the discharge, and it was necessary to throttle back on the cathode gas flow to reproduce the nominal discharge voltage at a given current. For example, in the TH15 mode, the nominal cathode flow rate is 3.7 sccm to operate at 25.5 V and 13.1 A. By injecting 1 sccm of gas into the plasma ball, it was possible to reduce the cathode gas flow to 0.8 sccm and maintain the nominal discharge voltage and current. It is clear that the majority of the gas injected through hollow cathodes is required for the generation of sufficient plasma exterior to the cathode in the near-cathode plume region (not inside the insert) to conduct the current to the anode. The lower cathode gas flow is then effective to reduce the internal pressure and increase the plasma contact area with the insert. The external gas injection was visually observed to create a more collimated plume near the cathode exit, which we named the jet mode, and reduced the radial extent of the plasma ball and the plasma fluctuation level. Figure 23 shows the radially positioned RPA data for this case. The number of high-energy ions is significantly reduced by the external gas injection that produces the jet-mode compared to the TH15 mode. This interesting discharge behavior and the resulting plasma properties are being further investigated at this time.[38]

VII. CONCLUSION

An investigation of the plasma parameters in the cathode insert, keeper, and anode regions of two different sized hollow cathodes used in NSTAR and NEXIS ion thrusters has been undertaken to determine the mechanism's high-energy ion production and keeper erosion. The RPA analyzer showed that a significant number of ions with energies well in excess of the discharge voltage were generated in or near the plasma ball just downstream of the keeper exit. While the RPA detected ions flowing in the radial direction in front of the keeper, it is likely that the same mechanism that produces these energetic ions (ionization at the peak of a potential oscillation and flowing down the potential gradient) will result in energetic ions flowing toward the keeper and eroding the electrode surfaces. Recent numerical modeling[27] supports this conclusion as the primary source of the observed keeper erosion.

Detailed measurements of the potential distributions throughout the discharge could not find a dc mechanism for acceleration of the significant number of ions to the high energies (>50 V) observed in these discharges under certain conditions. However, measurements of the rf plasma potential profile show fluctuations in the range of 50–1500 kHz

exist in the keeper region, with the largest amplitudes occurring at the edge of the plasma ball downstream of the cathode orifice in the keeper region. These oscillations range from ionization instabilities to turbulent ion acoustic waves, and can in some cases interact with the discharge power supply to cause gross unstable operation. The current of the high-energy ions collected by the RPA is consistent with the rf ion current measured by probes inserted into the plasma and the large-amplitude potential fluctuations. Detailed calculations of the keeper erosion using the high-energy ions from the measured rf fluctuations show that this mechanism fully explains the keeper erosion rates observed in the LDT and ELT life tests.[27] The results shown here indicate that with proper cathode/keeper design and proper selection of the cathode operating parameters, the plasma oscillations and high ion energies can be suppressed, which will reduce and hopefully mitigate excessive keeper wear.

ACKNOWLEDGMENTS

[1] A. T. Forrester, *Large Ion Beams* (Wiley-Interscience, New York, 1988).
[2] V. J. Friedly and P. J. Wilbur, J. Propul. Power **8**, 635 (1992).
[3] I. Kameyama and P. Wilbur, J. Propul. Power **16**, 529 (2000).
[4] G. Williams, T. B. Smith, M. T. Domonkos, A. D. Gallimore, and R. P. Drak, IEEE Trans. Plasma Sci. **28**, 1664 (2000).
[5] J. Foster and M. Patterson, J. Propul. Power **21**, 144 (2005).
[6] M. Croften and I. Boyd, *38th AIAA/ASME/SAE/ASEE Joint Propulsion Conference and Exhibit*, Indianapolis, IN, 2002, AIAA-2002-4103 (AIAA, Washington, D.C., 2002).
[7] J. R. Brophy and C. E. Gardner, *24th AIAA/ASME/SAE/ASEE Joint Propulsion Conference and Exhibit*, Boston, MA, 1988, AIAA-88-2913 (AIAA, Washington, D.C., 1988).
[8] M. Domonkos, J. Foster, and G. Soulas, J. Propul. Power **21**, 102 (2005).
[9] R. Kolasinski and J. Polk, *39th AIAA/ASME/SAE/ASEE Joint Propulsion Conference and Exhibit*, Huntsville, AL, 2003, AIAA-2003-5144 (AIAA, Washington, D.C., 2003).
[10] J. E. Polk, J. R. Anderson, J. R. Brophy, V. K. Rawlin, M. J. Patterson, J. Sovey, and J. Hamley, *35th AIAA/ASME/SAE/ASEE Joint Propulsion Conference and Exhibit*, Los Angeles, CA, 1999, AIAA-1999-2446 (AIAA, Washington, D.C., 1999).
[11] A. Sengupta, J. R. Brophy, J. R. Andreson, C. Garner, K. deGroh, T. Karniotis, and B. Banks, *40th AIAA/ASME/SAE/ASEE Joint Propulsion Conference and Exhibit*, Ft. Lauderdale, FL, 2004, AIAA-2004-3608 (AIAA, Washington, D.C., 2004).
[12] M. Patterson, V. K. Rawlin, J. S. Sovey, M. J. Kussmaul, and J. Parks, *31st AIAA/ASME/SAE/ASEE Joint Propulsion Conference and Exhibit*, San Diego, CA, 1995, AIAA-95-2516 (AIAA, Washington, D.C., 1995).
[13] J. R. Brophy, Rev. Sci. Instrum. **73**, 1071 (2002).
[14] I. Kameyama and P. Wilbur, *21st International Symposium on Space Technology and Science* (Sonic City, Omiya, Japan, 1998), ISTS Pap. No. 98-a-2-17.
[15] D. M. Goebel, K. Jameson, I. Katz, and I. Mikellades, J. Appl. Phys. **98**, 113302 (2005).
[16] K. Jameson, D. M. Goebel, and R. Watkins, *41st AIAA/ASME/SAE/ASEE Joint Propulsion Conference and Exhibit*, Tucson, AZ, 2005, AIAA-2005-3667 (AIAA, Washington, D.C., 2005).
[17] D. Herman and A. Gallimore, *41st AIAA/ASME/SAE/ASEE Joint Propulsion Conference and Exhibit*, Tucson, AZ, 2005, AIAA-2005-4251 (AIAA, Washington, D.C., 2005).
[18] J. E. Polk, D. M. Goebel, J. S. Snyder, L. Johnson, and A. Sengupta, *41st AIAA/ASME/SAE/ASEE Joint Propulsion Conference and Exhibit*, Tucson, AZ, 2005, AIAA-2005-4393 (AIAA, Washington, D.C., 2005).
[19] N. Hershkowitz and M. Cho, J. Vac. Sci. Technol. **6**, 2054 (1988).
[20] F. Chen, *Plasma Diagnostics Techniques* (Academic, New York, 1966), pp. 113–200.
[21] R. D. Kolasinski and J. E. Polk, J. Propul. Power **20**, 992 (2004).
[22] C. Farnell and J. Williams, 28th International Electric Propulsion Conference, Toulouse, France, 17–21 March 2003, IEPC-03-072.
[23] C. Farnell and J. Williams, *40th AIAA/ASME/SAE/ASEE Joint Propulsion Conference and Exhibit*, Ft. Lauderdale, FL, 2004, AIAA-2004-3432 (AIAA, Washington, D.C., 2004).
[24] D. Herman and A. Gallimore, *40th AIAA/ASME/SAE/ASEE Joint Propulsion Conference and Exhibit*, Ft. Lauderdale, FL, 2004, AIAA-2004-3958 (AIAA, Washington, D.C., 2004).
[25] A. Sengupta, *41st AIAA/ASME/SAE/ASEE Joint Propulsion Conference and Exhibit*, Tucson, AZ, 2005, AIAA-2005-4069 (AIAA, Washington, D.C., 2005).
[26] K. K. Jameson, K. Jameson, D. M. Goebel, and R. Watkins, 29th International Electric Propulsion Conference, Princeton University, 31 October–4 November 2005, IEPC-2005-269.
[27] I. G. Mikellides, I. Katz, D. M. Goebel, K. K. Jameson, and J. E. Polk, *43rd AIAA/ASME/SAE/ASEE Joint Propulsion Conference and Exhibit*, Cincinnati, OH, 2007, AIAA-2007-5192 (AIAA, Washington, D.C., 2007).
[28] I. I. Mikellades, I. Katz, D. M. Goebel, and K. K. Jameson, J. Appl. Phys. **101**, 063301 (2007).
[29] D. M. Goebel, J. E. Polk, and A. Sengupta, *40th AIAA/ASME/SAE/ASEE Joint Propulsion Conference and Exhibit*, Ft. Lauderdale, FL, 2004, AIAA-2004-3813 (AIAA, Washington, D.C., 2004).
[30] I. Mikellades, I. Katz, D. M. Goebel, and K. K. Jameson, J. Appl. Phys. **98**, 113303 (2005).
[31] I. Mikellades, I. Katz, D. M. Goebel, and K. K. Jameson, Phys. Plasmas **13**, 063504 (2006).
[32] D. M. Goebel, K. Jameson, I. Katz, I. Mikellides, and J. Polk, 29th International Electric Propulsion Conference, Princeton University, 31 October–4 November 2005, IEPC-2005-266.
[33] J. P. Boeuf and L. Garrigues, J. Appl. Phys. **84**, 3541 (1998).
[34] H. R. Kaufman, "Technology of electron-bombardment ion thrusters," in *Advances in Electronics and Electron Physics*, edited by L. Marton (Academic, New York, 1974), Vol. 36, p. 354.
[35] T. M. Jack, S. W. Patterson, and D. G. Fearn, *36th AIAA/ASME/SAE/ASEE Joint Propulsion Conference and Exhibit*, Huntsville, AL, 2000, AIAA-2000-3533 (AIAA, Washington, D.C., 2000).
[36] R. H. Martin, C. C. Farnell, and J. Williams, 29th International Electric Propulsion Conference, Princeton, NJ, 31 October–4 November 2005, IEPC 2005-294.
[37] I. Katz, I. G. Mikellides, D. M. Goebel, K. K. Jameson, and J. E. Polk, *42nd AIAA/ASME/SAE/ASEE Joint Propulsion Conference and Exhibit*, Sacramento, CA, 2006, AIAA-2006-4485 (AIAA, Washington, D.C., 2006).
[38] D. M. Goebel, K. Jameson, I. Katz, I. Mikellides, and J. Polk, 30th International Electric Propulsion Conference, Florence, Italy, 17–20 September 2007, IEPC-2007-277.